Firn data compilation reveals the evolution of the firn air content on the Greenland ice sheet

Baptiste Vandecrux[1,2], Michael MacFerrin[3], Horst Machguth[4, 5], William T. Colgan[1], Dirk van As[1], Achim Heilig[6], C. Max Stevens[7], Charalampos Charalampidis[8], Robert S. Fausto[1], Elizabeth M. Morris[9], Ellen Mosley-Thompson[10], Lora Koenig[11], Lynn N. Montgomery[11], Clément Miège[12], Sebastian B. Simonsen[13], Thomas Ingeman-Nielsen[2], Jason E. Box[1]

[1] Department of Glaciology and Climate, Geological Survey of Denmark and Greenland, Copenhagen, Denmark.
[2] Department of Civil Engineering, Technical University of Denmark, Lyngby, Denmark.
[3] Cooperative Institute for Research in Environmental Sciences, University of Colorado, Boulder, CO USA
[4] Department of Geosciences, University of Fribourg, Fribourg, Switzerland
[5] Department of Geography, University of Zurich, Zurich, Switzerland
[6] Department of Earth and Environmental Sciences, LMU, Munich, Germany
[7] Department of Earth and Space Sciences, University of Washington, WA USA
[8] Bavarian Academy of Sciences and Humanities, Munich, Germany
[9] Scott Polar Research Institute, Cambridge University, United Kingdom
[10] Byrd Polar and Climate Research Center and Department of Geography, Ohio State University, Columbus, OH USA.
[11] National Snow and Ice Data Center, University of Colorado, Boulder, CO, United States
[12] Department of Geography, Rutgers University, Piscataway, NJ, United States
[13] DTU Space, National Space Institute, Department of Geodynamics, Technical University of Denmark, Kgs. Lyngby, Denmark

Correspondence to: B. Vandecrux (bava@byg.dtu .dk)

Abstract. The firn covering the Greenland ice sheet interior can retain part of the surface melt each summer, buffering the ice sheet contribution to sea-level rise. To quantify the firn meltwater retention capacity, we derive from 360 firn observations the Firn Air Content in the top 10 m (FAC_{10}) and in the entire firn column (FAC_{tot}). We then map the FAC over the entire firn area using empirical functions of long-term mean air temperature ($\overline{T_a}$) and net snow accumulation ($\bar{b}$) fitted to observations. We find that the firn layer contains a total 26 800 ±1 850 km^3 of air, with 6 500 ± 450 km^3 in the top 10 m. The FAC was stable between 1953 and 2017 in the dry snow area ($\overline{T_a}$ ≤-19°C), while it decreased by 24 ±16% in the low accumulation wet snow area ($\overline{T_a}$>-19°C $\bar{b}$ ≤ 600 mm w.eq. yr^{-1}) between 1997-2008 and 2011-2017 leading to a loss of firn retention capacity between 150 ± 100 Gt (top 10 m) and 540 ± 450 Gt (whole firn column). The outputs of three regional climate models (HIRHAM5, RACMO2.3p2, MAR3.9) compare well with observed FAC_{10}. However model biases in FAC_{tot} and other mismatches with our dataset urge caution when using models to quantify the current and future evolution of the firn air content and retention capacity.

1. Introduction

As a consequence of anthropogenic carbon emissions and subsequent atmospheric and oceanic warming, the Greenland ice sheet is losing mass at an accelerating rate, and contributes to about 20% of contemporary sea-level rise (Bindoff et al., 2013; Nerem et al. 2018). Over half of this mass loss stems from surface melt occurring every summer at the surface of the ice sheet and meltwater runoff to the ocean (van den Broeke et al., 2016). While most runoff originates from the low-lying ablation area, surface melt has recently increased and expanded up-glacier into the firn-covered interior of the Greenland ice sheet (Mote et al. 2007, Nghiem et al., 2012). Yet, most of the surface meltwater produced in firn-covered regions percolates into the snow and firn where it refreezes, and does not immediately contribute to sea-level rise (Harper et al., 2012). Hence the retention capacity of the firn area of the Greenland ice sheet constitutes a key parameter in sea-level equation.

The firn area extent can be tracked using the firn line, which Benson (1962) described as "the highest elevation to which the annual snow cover recedes during the melt season". Recently Fausto et al. (2018a) updated the methods from Fausto et al. (2007) and presented maps of remotely-sensed end-of-summer snowlines over the 2000-2017 period that can be used to map the firn area.

A second key characteristic for the retention of meltwater is the firn air content (FAC). The FAC is the integrated volume of air contained in the firn from the surface to a certain depth per unit area (van Angelen et al., 2012; Ligtenberg et al., 2018). It is a measure of the firn porosity and indicative, for a specified depth range, of the maximum volume available to store percolating meltwater either in liquid or refrozen form (Harper et al., 2012; van Angelen et al. 2012). While the role of FAC in meltwater retention has long been recognized, insufficient data from the firn area in Greenland made it necessary, until lately, to use simplifying assumptions (e.g. Pfeffer et al., 1991) or unvalidated outputs from regional climate model (RCM, van Angelen et al., 2013) to constrain the firn's meltwater retention capacity. Harper et al., (2012) gave a first observation-based estimate of this retention capacity of the ice sheet percolation area. Their approach was limited by the use of observations from two years (2007 and 2008) and 15 sites along the western slope of the ice sheet without regards to the diversity of firn characteristics across the ice sheet (e.g. Forster et al. 2014; Machguth et al., 2016). More recently, Ligtenberg et al. (2018) provided a RCM simulation of the FAC which compared well against 62 firn cores. Nevertheless, their FAC simulation still underestimated FAC in the lower accumulation area. Focusing on meltwater percolation, Langen et al. (2017) also compared how the output of HIRHAM5 RCM compared against 75 firn density profiles while its FAC has not been investigated.

The depth to which meltwater may percolate, and therefore the depth to which FAC must be calculated to constrain the firn's meltwater retention capacity, varies with melt intensity and firn permeability (e.g. Pfeffer et al., 1991). Braithwaite et al. (1994) reported meltwater refreezing within the top 4 m of the firn in western Greenland at ~1500 m a.s.l. while Heilig et al.

(2018) did not observe meltwater percolation below 2.3 m from the surface throughout 2016 melt season, at 2120 m a.s.l. also in west Greenland. Both studies indicate that, at specific sites and years, only the near-surface FAC was being used to store meltwater. However, in 2007-2009 ~400 km to the north and at 1555 m a.s.l., Humphrey et al. (2012) observed percolation below 10 m, meaning that, for certain firn temperature and stratigraphy and given sufficient surface meltwater, the FAC of the whole firn column, from the surface to pore-close-off depth, might be used for meltwater retention. Nevertheless, Machguth et al. (2016) showed that percolation depth may not increase linearly with meltwater production and that low-permeability ice layers can limit meltwater, even if abundant, from accessing the full firn column. Given the complexity of meltwater percolation and the limited observations to map percolation depth on the Greenland ice sheet, reasonable upper and lower bounds of the firn's capacity can be estimated by determining both the FAC in the top 10 m of firn (FAC_{10}) and the total FAC (FAC_{tot}) (Harper et al. 2012). FAC_{tot} is also valuable information to convert remotely-sensed Greenland ice sheet surface height changes into mass changes (Simonsen et al. 2013; Sørensen et al., 2011, Kuipers Munneke et al. 2015a).

In this study, we first estimate the firn area extent using remotely-sensed end-of-summer snow extent maps from Fausto et al. (2018a). We then use a set of 360 firn observations collected between 1953 and 2017 to calculate the spatial distribution of FAC_{10} and where possible present its temporal evolution. A simple extrapolation is introduced to estimate the FAC_{tot} from the FAC_{10}. By spatially integrating FAC_{10} and FAC_{tot} over the firn area, we calculate the lower and upper bounds of the firn retention capacity. Finally, we evaluate the performance of firn simulations in three regional climate models (RCMs), commonly used to evaluate firn retention capacity, but never validated with such extensive firn data collection.

2. Data and methods

2.1. Firn core dataset

We gathered 324 published firn-density profiles from cores that were at least 5 m long (Table 1). To these, we add 20 cores extracted in April-May 2016 and 2017 for which the density was measured at 10 cm resolution following the same procedure as Machguth et al. (2016). Most of these density profiles are available in Montgomery et al. (2018). When near-surface snow densities were missing, we assigned a density of 315 kg m^{-3} (Fausto et al., 2018b) to the top cm and interpolate over the remaining gaps in density profiles using a logarithmic function of depth fitted to the available densities.

Table 1. List of the publications presenting the firn cores used in this study.

Source	Number of cores	Source	Number of cores
Albert and Shultz (2002)	1	Langway (1967)	1
Alley (1987)	1	Lomonaco et al. (2011)	1

Bader (1954)	1
Baker (2012)	1
Benson (1962)	55
Bolzan and Strobel (1999)	9
Buchardt et al. (2012)	8
Clausen et al. (1988)	8
Colgan et al. (2018)	1
Fischer et al. (1995)	14
Forster et al. (2014)	5
Hawley et al. (2014)	8
Harper et al. (2012)	32
Jezek (2012)	1
Kameda et al. (1995)	1
Koenig et al. (2014)	3
Kovacs et al. (1969)	1

Machguth et al. (2016)	28
Mayewski and Whitlow (2016a)	1
Mayewski and Whitlow (2016b)	1
Miège et al. (2013)	3
Morris and Wingham (2014)	66
Mosley-Thompson et al. (2001)	47
Porter and Mosley-Thompson (2014)	1
Reed (1966)	1
Renaud (1959)	7
Spencer et al. (2001)	8
Steen-Larsen et al. (2011)	1
Vallelonga et al. (2014)	1
van der Veen et al. (2001)	10
Wilhelms (1996)	13
This study	20

In addition to our collection of firn density, we use the end-of-summer snowlines from Fausto et al. (2018a) to delineate the minimum firn area, which are the 1,405,500 km^2 where snow is always detected during the 2000-2017 period. Moving this firn line 1 km inward or outward (the resolution of the product from Fausto et al. (2018a)) suggest an uncertainty of ±17,250 km^2 (~1%). This uncertainty applies on the margin of the firn area where ephemeral or thinner firn patches may exist outside of our delineation. Owing to the likely thinness of the accumulation area lower boundary, we expect the boundary does not play a negligible role in the overall retention capacity of the firn area.

2.2. Calculation of FAC_{10}

For a discrete density profile composed of N sections and reaching a depth z, the FAC in m is calculated as:

$$FAC_z = \sum_{k=1}^{N} m_k \left(\frac{1}{\rho_k} - \frac{1}{\rho_{ice}}\right) \quad [1]$$

where, for each depth interval k, ρ_k is the firn density and m_k is the firn mass. ρ_{ice} is the density of the ice set to 917 kg/m^3.

With 121 cores shorter than 10 m in our dataset, we extrapolate shallow measurements to a depth of 10 m. We do this by finding the 10 m long core that best matches the FAC vs. depth profile of the shallow core, with the lowest Root Mean Squared Difference (RMSD) amongst all available cores, and append the bottom section of this 'twin' core to the FAC profile of the shallow core (see Figure S1 of the Supplementary Material). When testing this methodology on the available

cores deeper than 10 m, from which we remove the deepest 3 m of the FAC profile, we find a mean difference between extrapolated and real FAC_{10} inferior to 1% and a RMSD of 0.15 m.

The accuracy of the firn density measurements as well as the effect of spatial heterogeneity can be assessed by comparing FAC_{10} measurements located within 1 km and collected in the same year (Figure S2 of the Supplementary Material). A standard deviation below 0.15 m is found in the majority of the co-located and contemporaneous FAC_{10} observations (20 of 27 groups of comparable observations). We assign to FAC_{10} measurements an uncertainty of $\pm$0.3 m, i.e., twice the standard deviation.

2.3. Zonation of firn air content

The FAC_{10} is calculated from the firn density which depends, among other parameters, on the local near-surface air temperature and snowfall rate (Shumskii, 1964). The site's air temperature is a proxy for summer melt and refreezing within the firn, as well as firn temperature and compaction rates. Through these processes, air temperature has a lowering effect on FAC_{10}. On the other hand, snow accumulation introduces porous fresh snow at the surface and has an increasing effect on FAC_{10}. To put our FAC_{10} measurements in their climatic context, we extract the long-term (1979-2014) average net snow accumulation $\dot{b}$ (snowfall – sublimation) and air temperature $\overline{T_a}$ for each FAC_{10} measurement location from the nearest cell in the Modèle Atmosphérique Régional (MARv3.5.2; Fettweis et al., 2017) available at 5 × 5 km horizontal resolution.
In accordance with the terminology from Benson (1962), we define three regions where FAC_{10} shows distinct behaviour: (1) the dry snow area (DSA, yellow area in Figure 1a); (2) the low accumulation wet snow area (LAWSA, red area in Figure 1a); (3) the high accumulation wet snow area (HAWSA, green area in Figure 1a). The DSA encompasses low temperature regions of high altitude and/or latitude where melt is uncommon and where FAC_{10} can be related by a linear function of $\overline{T_a}$ (yellow markers in Figure 1c). Towards higher $\overline{T_a}$, i.e. at lower altitude and/or latitude, two patterns are visible in Figure 1c. Firstly, at lower $\bar{b}$ sites, in the LAWSA, more scatter appears in FAC_{10}, and a slope change occurs in the FAC_{10}'s temperature dependency (Figure 1c). Secondly, at higher $\bar{b}$ (in the HAWSA), the few available FAC_{10} observations describe a similar temperature dependency as in the DSA even though they are in relatively warm regions where melt occurs more frequently and cannot be referred to as "dry". FAC_{10} observations in the HAWSA are up to five times higher than at locations with similar $\overline{T_a}$ in the LAWSA (Figure 1c).

The boundary between the cold (DSA) and warm regions (LAWSA and HAWSA) can be defined as the temperature where an inflection occurs in the linear dependency of FAC_{10} to $\overline{T_a}$ (Figure 1c). The transition between areas, just as between the facies described by Benson et al. (1962), is gradual, but for our analysis, we set this boundary to $\overline{T_a}$ = -19 °C. No firn observation is available in the transition from the LAWSA to the HAWSA. A boundary could be anywhere between 543 mm

w.eq./yr (core with highest accumulation in the LAWSA, Figure 1b) and 650 mm w.eq. yr^{-1} (core with lowest accumulation in HAWSA, Figure 1b). We chose the rounded value of $\bar{\dot{b}}$ = 600 mm w.eq. yr^{-1} to separate LAWSA from HAWSA. The spatial delineations of the DSA, LAWSA and HAWSA are illustrated in Figure 1a.

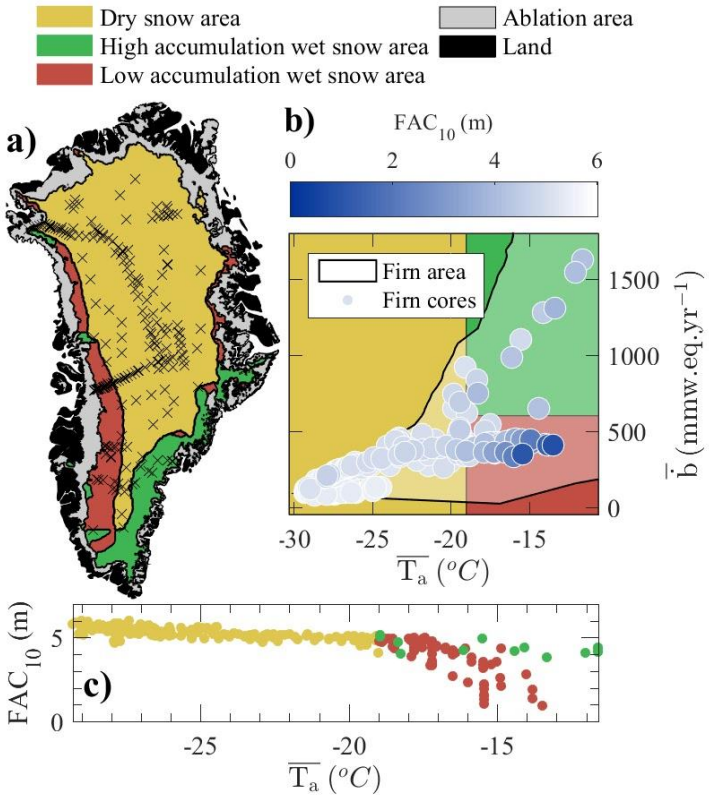

Figure 1. a) Spatial distribution of the FAC_{10} dataset. The DSA, LAWSA and HAWSA are indicated respectively using yellow, green and red areas. b) Distribution of the dataset in the accumulation-temperature space ($\bar{\dot{b}}$ and $\overline{T_a}$). FAC_{10} value is indicated by a coloured marker. Black lines and shaded areas indicate where the firn is detected in the accumulation-temperature space. c) Temperature dependency of FAC_{10} in the DSA (yellow markers), LAWSA (red markers) and HAWSA (green markers).

2.4. Firn air content mapping

To map FAC_{10} over the entire firn area, we fit empirical functions to the FAC_{10} observations and use these functions to spatially interpolate and extrapolate FAC_{10}. The construction of these empirical functions is described in the following sections and an overview of their form and their associated data is presented in Table 2.

Table 2. Overview of the empirical functions fitted to FAC_{10} observations in each region of the firn area.

Area	Period	Form	Observations used for fitting

DSA	1953 - 2017	Linear function of $\overline{T_a}$ (Eq. 2)	259 from the DSA 11 from the HAWSA
LAWSA & HAWSA	2010 - 2017	• Smoothed bilinear function of $\overline{T_a}$ and $\bar{b}$. • Cannot exceed the FAC estimated with Eq. 2.	25 from the LAWSA 10 from the HAWSA 6 selected from firn line in the HAWSA
LAWSA	1998 - 2008		38 from the LAWSA 1 from the HAWSA 6 selected from the firn line in the HAWSA

2.4.1. Dry Snow Area

In the DSA, the 259 FAC_{10} observations obtained between 1953 and 2017 depend linearly on their local $\overline{T_a}$ (Figure 1c). This dependency is the same for the 11 FAC_{10} observations from the HAWSA. We consequently use a linear function of $\overline{T_a}$ fitted using least squares method to the FAC_{10} observed in both DSA and HAWSA (Figure 2a) binned into four equal $\overline{T_a}$ ranges (to avoid the overrepresentation of clustered data) to estimate the FAC_{10} in the DSA.

2.4.2. Wet Snow Areas

In the LAWSA and in the HAWSA, FAC_{10} observations exhibit a more complex dependency to $\bar{b}$ and $\overline{T_a}$ (Figure 1b and 1c). Additionally, observations are unevenly distributed in space and time which forces us to group FAC_{10} measurements into time-slices that contain enough FAC_{10} observations to describe the spatial pattern of FAC_{10} and constrain our empirical functions.

Over the 2010-2017 period, 25 FAC_{10} observations were made in the LAWSA, from the transition with the DSA down to the vicinity of the firn line. During that same period, 10 firn cores were collected in the HAWSA. Unfortunately, in addition to their small number, the cores are located relatively far into the interior of the ice sheet and do not describe how the FAC_{10} decreases in parts of the HAWSA closer to the firn line. We consequently complement these firn cores with 6 sites selected on the remotely-sensed firn line where FAC_{10} is assumed to be null (Figure S3).

We define our empirical function, valid in the LAWSA and HAWSA for the 2010-2017 period, as a smoothed bilinear function of $\overline{T_a}$ and $\bar{b}$ fitted through least squares method to the available observations (Figure 3a). We do not allow that function to exceed the linear function of $\overline{T_a}$ that describes FAC_{10} measurements in the DSA and in the interior of the

HAWSA or to predict FAC_{10} below 0 m. The empirical function is then used to estimate the FAC_{10} in both the LAWSA and HAWSA during the 2010-2017 period.

In the years preceding 2010, insufficient data are available to document the FAC_{10} in the HAWSA. In the LAWSA, however, 34 observations were made between 2006 and 2008 and three cores were collected in 1998. We group these measurements to describe the spatial distribution of FAC_{10} in the LAWSA during the 1998-2008 period and to fit another function, this time only valid in the LAWSA during the 1998-2008 period, also smoothed bilinear function of $\overline{T_a}$ and $\bar{\dot{b}}$. To ensure that our empirical function has realistic values towards the transition with the HAWSA, we also include one core collected in the HAWSA in 1998 and the previously described six locations from the firn line in the fitting process (Figure 3a).

We investigate the robustness of our empirical functions in the HAWSA and LAWSA using, for each period separately, the following sensitivity analysis. For 1000 repetitions, we apply four types of perturbations to the FAC_{10} observations and fit our empirical function to this perturbed dataset. The effect of the availability of measurements in the LAWSA is tested by randomly excluding four observations in that region (respectively 16% and 11% of the observations in 1998-2008 and 2010-2017). The effect of uncertainty in the firn line location in the $\left(\overline{T_a}, \bar{\dot{b}}\right)$ space is tested by adding a normally distributed noise with mean zero and standard deviation 3 $^{\circ}$C to the $\overline{T_a}$ of firn-line-derived FAC_{10} (illustrated in Figure S3). The effect of the uncertain FAC_{10} value at the firn line is assessed by assigning to the points selected from the firn line a random FAC_{10} value between 0 and 1 m. Finally, the effect of the smoothing applied to the bilinear interpolation of FAC_{10} measurements is assessed by modifying the amount of smoothing applied. We then calculate the standard deviation of all possible estimated FAC_{10} at each $\left(\overline{T_a}, \bar{\dot{b}}\right)$ location and double it to quantify the 95% envelope of uncertainty that applies to any estimated FAC_{10} in the LAWSA and HAWSA depending on $\left(\overline{T_a}, \bar{\dot{b}}\right)$. We do not consider that the uncertainty applying on an estimated FAC_{10} can be smaller than the one of FAC_{10} observations. We consequently set 0.3 m as the minimum possible uncertainty on any estimated FAC_{10}.

2.5. Estimation of the FAC_{tot}

While FAC_{tot} may be calculated from the surface down to pore close off depth (Ligtenberg et al., 2018), to allow comparison with HIRHAM5 which sometimes do not reach pore close off, we calculate FAC_{tot} from the surface to 100 m depth. Only 29 of our 360 firn observations reach depths greater than 100 m so we complement them by 13 observations from Harper et al. (2012) that estimated FAC_{tot} at their core sites from ground penetrating radar. A linear function is fitted to these data and is used to estimate FAC_{tot} at the rest of our FAC_{10} observation sites.

2.6. Spatially integrated FAC, uncertainty and retention capacity

For each region, the spatially integrated FAC is the sum of the entire firn air volume either within the top 10 m or in the whole firn column. The uncertainty applying on our estimated FAC_{10} and FAC_{tot} at a location cannot be considered independent because all estimates are made using the same functions of $\overline{T_a}$ and $\bar{\dot{b}}$. Consequently, we consider that the uncertainty of the mean of several FAC values is the mean of each value's uncertainty and that the uncertainty of a sum or difference of FAC values is the sum of the uncertainty applying on these FAC values.

From the FAC, we calculate the firn's maximum retention capacity, which Harper et al. (2012) defined as the amount of water that needs to be added to the firn to bring its density to 843 kg m^{-3}, the density of infiltration ice.

2.7. Comparison with Regional Climate Models

We compare our FAC observations and maps to the available firn products from three RCMs: HIRHAM5, RACMO2.3p2 and MARv3.9. The two versions of HIRHAM5 presented in Langen et al. (2017) are used: with linear parametrization of surface albedo (thereafter referred as HH_LIN) and MODIS-derived albedo (thereafter referred as HH_MOD). Because of model output limitation, only FAC_{tot} could be extracted from the RACMO2.3p2 output presented by Ligtenberg et al. (2018) and the FAC_{10} was extracted from the more recent downscaled model output by Noël et al. (2019). MARv3.9 was presented in Fettweis et al. (2017) and simulates only FAC_{10} because of a shallower subsurface domain.

3. Results and Discussion

3.1. FAC estimation

3.1.1. Dry snow area

In the DSA, the linear function of $\overline{T_a}$ used to estimate FAC_{10} reads as:

$$FAC_{10}(\overline{T_a}) = -0.08 * \overline{T_a} + 3.27 \quad [2]$$

We assign to any FAC_{10} estimated in the DSA an uncertainty equal to twice the regression's RMSD: 0.4 m. We consider the absence of a temporal trend in the deviation between measured FAC_{10} and FAC_{10} estimated using the linear function of $\overline{T_a}$ (Figure 2b) as evidence of the stability of the FAC_{10} in the DSA between 1953 and 2017. The stable FAC in the DSA is confirmed by firn cores in our dataset taken decades apart at the same sites and showing the same FAC (Summit, Camp Century, e.g.) and by recent firn modelling at weather stations located in the DSA (Vandecrux et al. 2018).

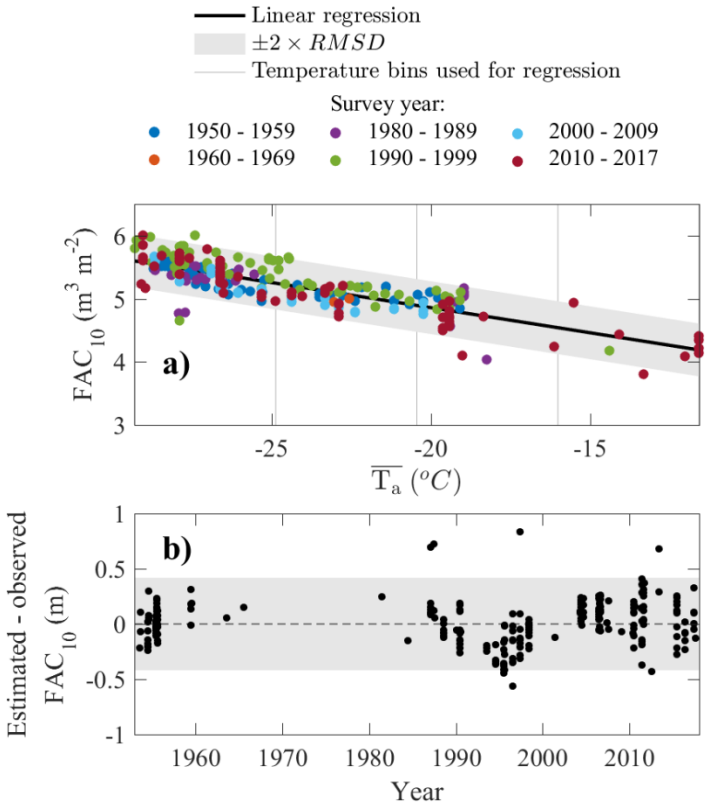

Figure 2. a) Linear function of $\overline{T_a}$ fitted to FAC_{10} observations from the DSA and HAWSA. b) Residual between estimated (using linear regression) and observed FAC_{10} as a function of survey year.

3.1.2. Wet snow areas

In the LAWSA and HAWSA, we estimate the FAC_{10} with the empirical functions presented in Figure 3. These empirical functions have a RMSD of 0.28 m in the LAWSA over the 1998-2008 period, 0.27 m in the LAWSA over the 2010-2017 period and 0.17 m in the HAWSA over the 2010-2017 period. The ability of our empirical functions to fit the FAC_{10} observations confirms our choice of an empirical approach as opposed to relying on RCMs and firn models which still do not accurately reproduce observations of FAC in certain regions (see Section 3.6).

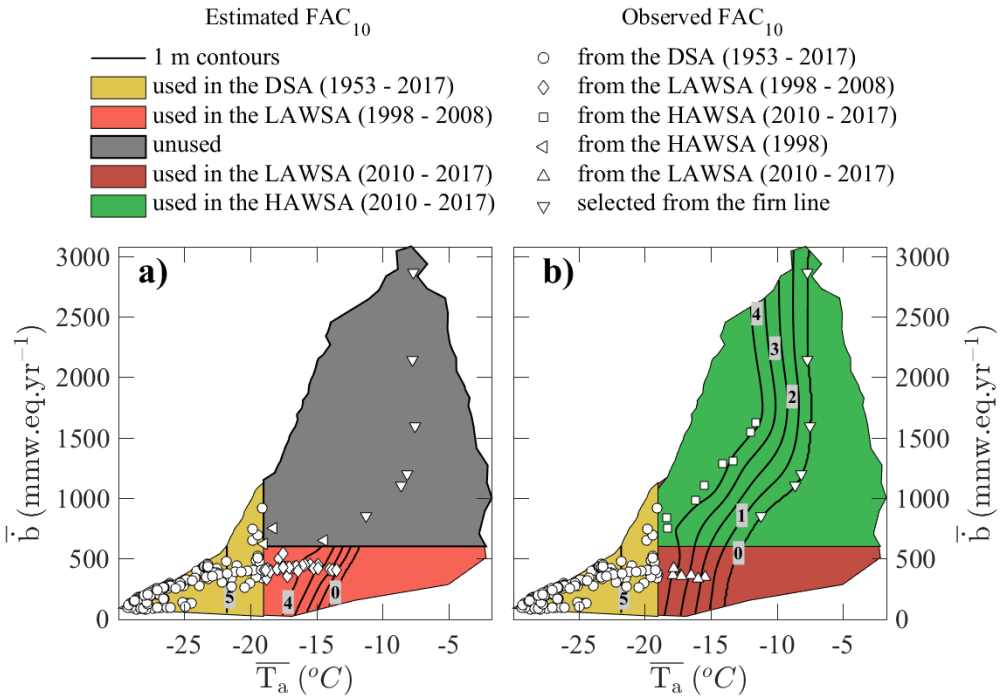

Figure 3. Contours (labelled black lines) of the empirical functions of $\overline{T_a}$ and $\overline{\dot{b}}$ used to estimate FAC_{10} along with the FAC_{10} observations used to constrain the functions. Two functions could be constructed: one describing FAC_{10} in the LAWSA during 1998-2008 (a) and another describing FAC_{10} in the LAWSA and HAWSA during 2010-2017 (b).

3.1.3. FAC_{tot}

We use the following linear regression between FAC_{10} and FAC_{tot} (Figure 4):

$$FAC_{tot} = 4.1 * FAC_{10} \quad [3]$$

We assign 3.6 m, twice the RMSD of the linear regression, as the typical uncertainty applying on an estimated FAC_{tot} value, representing less than 20% of estimated FAC_{tot} greater than 20 m but up to 100% of the estimated FAC_{tot} at the firn line.

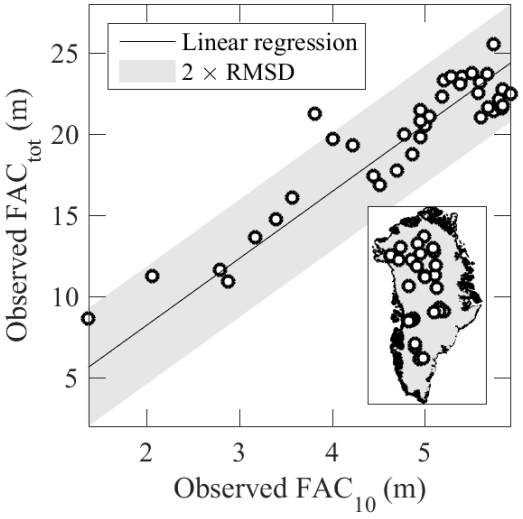

Figure 4. Linear regression used to estimate FAC_{tot} from FAC_{10}. Linear regression was fitted using the least squares method with a prescribed intercept of zero.

One of the consequences of Eq. 2 is that a change FAC_{10} between two dates implies a change in FAC_{tot} over the same time period. This co-variation neglects that near-surface changes in the firn slowly propagate to greater depth with thermal conduction and downward mass advection (Kuipers Munneke et al., 2015b). Therefore we note that for a decreasing FAC_{10} (see Section 3.2.1), our estimated change in FAC_{tot} will always be the maximum possible change, if the whole firn column was given the time to adapt to the new surface conditions.

3.2. Spatio-temporal distribution of firn air content

3.2.1. FAC_{10} mapping

Using the 5x5 km $\overline{T_a}$ and $\bar{\dot{b}}$ grids from Fettweis et al. (2017) and the empirical functions presented in Figure 3, we map the FAC_{10} and its uncertainty across the firn area of the ice sheet (Figure 5). From these maps we calculate an average FAC_{10} of 5.1± 0.3 m in the DSA, an average FAC_{10} of 2.6 ± 0.5 m in the HAWSA during the 2010-2017 period and an average FAC_{10} of 4 ± 0.3 m in the LAWSA during the 1998-2008 period, which decreased by 35 % to 2.6 ± 0.3 m in the 2010-2017 period. The FAC_{10} loss in the LAWSA is concentrated in a 60 km wide band above the firn line in western Greenland (Figure 6).

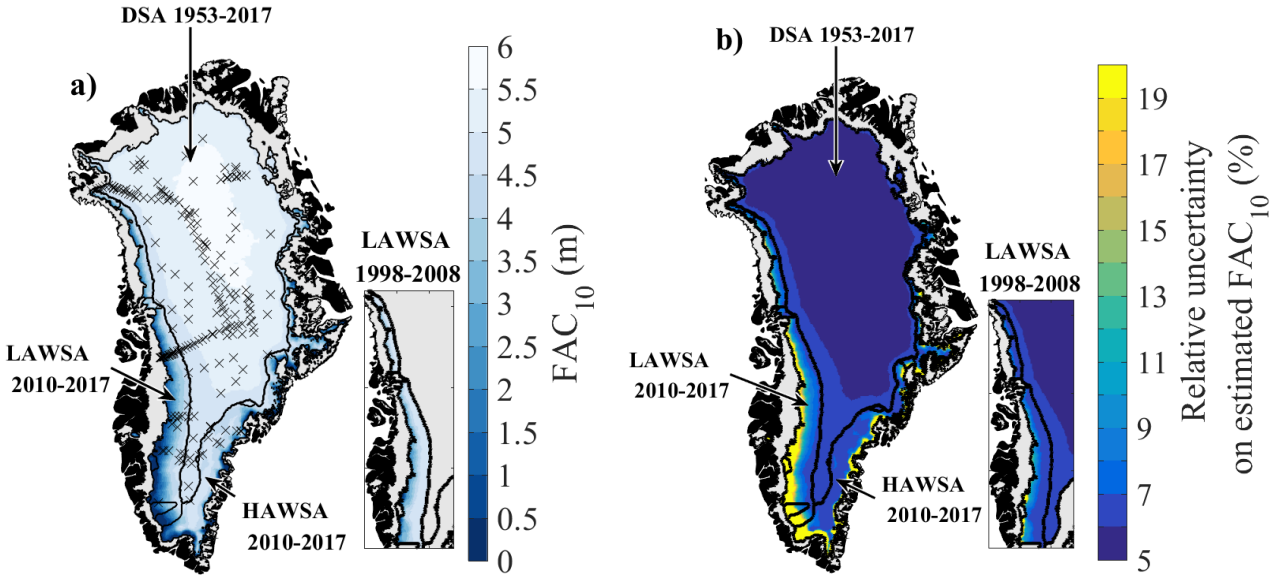

Figure 5. a) FAC_{10} maps and location of the FAC_{10} measurements. b) Maps of the relative uncertainty of the FAC_{10} map.

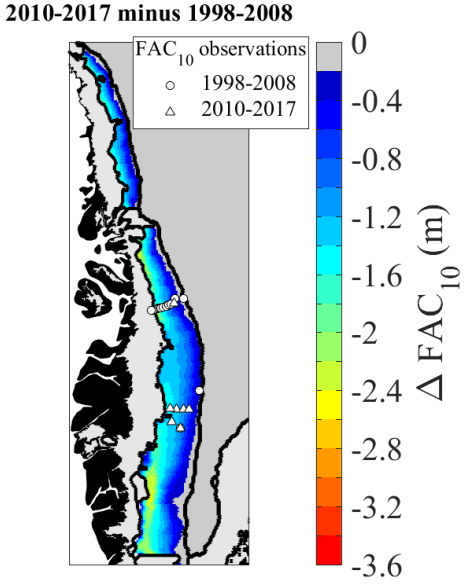

Figure 6. Change in FAC_{10} between 1998-2008 and 2010-2017 in the LAWSA.

3.2.2. Spatially integrated FAC

We find that during the 2010-2017 period the entire firn area contains 6 500 ± 450 km^3 in the top 10 m and up to 26 800 ± 1 850 km^3 if the whole firn column is accounted for (Table 3). About 83 ± 5% of this air content is contained in the DSA,

which represents 74% of the firn area. The HAWSA, which covers 12% of the firn area, contains about 8 ± 1% of the firn's air independently of whether we consider the top 10m or at the entire firn layer.

Table 3. Spatially integrated FAC_{10} and FAC_{tot} over each ice sheet region

Area	Period	Spatially integrated FAC (km^3)					
		FAC_{10}			FAC_{tot}		
DSA	1953 – 2017	5 400	±	310	22 300	±	1 280
LAWSA	1998 – 2008	750	±	60	3 100	±	250
LAWSA	2010 – 2017	570	±	60	2 400	±	250
HAWSA	2010 – 2017	530	±	80	2 200	±	330
All	2010 – 2017	6 500	±	450	26 800	±	1 850

In the LAWSA, that comprises 14 % of the firn area, decreasing FAC_{10} between 1998-2008 and 2010-2017 lead to a loss of 180 ± 120 km^3 of air from the top 10 m of firn, equivalent to 24 ± 16% of the 1998-2008 spatially integrated FAC_{10}. The subsequent decrease in FAC_{tot} indicate that the whole firn column lost up to 700 ± 500 km^3 of air.

Recent studies attributed the increasing near-surface firn densities and subsequent loss of FAC to increasing surface melt and meltwater refreezing (de la Peña et al., 2015; Charalampidis et al., 2015; Machguth et al., 2016; Graeter et al., 2018). However, firn density and FAC are also dependant on annual snowfall and a decrease in snowfall can drive an increase in firn density and consequently a decrease in FAC_{10} (e.g. Vandecrux et al., 2018). Nevertheless, the lack of widely distributed observation of snow accumulation for the 1998-2017 period and the contradicting trends in precipitation output by the RCMs (Lucas-Picher et al., 2012; van den Broeke et al., 2016; Fettweis et al., 2017) make it impossible to precisely partition the melt and snowfall contributions to changes in FAC_{10} at ice sheet scale.

3.2.3. Effect of the $\overline{\dot{b}}$ and $\overline{T_a}$ data source FAC_{10} maps

To investigate how uncertainties in $\overline{T_a}$ and $\overline{\dot{b}}$ impact our FAC_{10} maps, we repeat our procedure using the 1979-2014 $\overline{T_a}$ and $\overline{\dot{b}}$ estimated by Box (2013) and Box et al. (2013) (hereafter referred to as "Box"). The Box-derived FAC_{10} fits equally well (within measurements uncertainty, RMSD < 0.3 m) to the FAC_{10} observations and lead to spatially integrated FAC values within uncertainty from the MAR-derived values (Table 3).

However, due to differing model formulations and forcing, the spatial patterns of air temperature and snowfall are different between Box and MARv3.9.2 (detailed in Fettweis et al. 2017), especially in the southern and eastern firn area, which leads to different estimations of FAC_{10} in these regions (Figure S4). Additionally, in these regions no firn observations are

available to constrain our FAC_{10} estimates. More observations in the sparsely observed southern and eastern regions would therefore not only improve FAC_{10} estimates, but also elucidate which $\overline{T_a}$ and $\bar{\dot{b}}$ source best describes the spatial pattern in FAC_{10}.

3.3. Firn retention capacity

Between 1998-2008 and 2010-2017, the decrease in FAC_{10} in the LAWSA indicates a 150 ± 100 Gt, or 0.4± 0.3 mm sea level equivalent (s.l.e.), loss of meltwater retention capacity from the top 10 m of the firn. For the entire firn column, we estimate a loss could be up to 540 ± 450 Gt (1.5 ± 1.2 mm s.l.e.). While these volumes are small as compared to the average mass loss of the ice sheet (~270 Gt/y), the impact of reduced retention capacity has an important time-integrated effect, in amplifying meltwater runoff each year, especially in a succession of anomalously high melt years as was the case 2007-2012, resulting in a sharp increase in western Greenland runoff (Machguth et al. 2016).

Table 4. Firn storage capacity for the top 10 m and for the entire firn column

Area	Period	Firn storage capacity (Gt)					
		Upper 10 m			Whole firn column		
DSA	1953 – 2017	4 200	±	370	12 800	±	1 170
LAWSA	1998 – 2008	550	±	50	1 490	±	220
LAWSA	2010 – 2017	400	±	50	950	±	230
HAWSA	2010 – 2017	370	±	70	960	±	300
All	2010 – 2017	5 000	±	410	14 700	±	1 600

Harper et al. (2012), using observations from 2007-2009, estimated that the firn located in a 150 000 km^2 percolation area (as delineated in an earlier version of MAR) could potentially store between 322 ±44 Gt in the top 10 m of firn and $1\ 289\ ^{+388}_{-252}$ Gt if considering the entire firn column. We find that the warmest 150 000 km^2 of our firn area in 2010-2017 can retain 150 ± 67 Gt of meltwater in the top 10 m of the firn. When considering the whole firn layer we find a storage capacity of 310 Gt associated with an uncertainty of 688 Gt. Our lower estimated retention capacity reflects the recent decrease of FAC in the LAWSA. Interestingly, we reach equivalent uncertainty intervals than Harper et al. (2012) in spite of using ~20 times more firn observations. We also note that the estimation from Harper et al. (2012) only used observations in the LAWSA, while most (69%) of the percolation area they use is located in the HAWSA. Finally, our distributed approach, as opposed to the lumped approach of Harper et al. (2012), now makes it possible to determine, given a certain melt extent, how much of the firn retention capacity is available to store meltwater.

Both our estimated retention capacity and the one of Harper et al. (2012) use the same infiltration ice density, 843 ± 36 kg m^{-3}, which was measured in portions of firn cores saturated by refrozen meltwater. In a later study also in western Greenland, Machguth et al. (2016) measured an infiltration ice density of 873 ±25 kg m^{-3}. Using the value from Machguth et al. (2016) increases our estimated firn storage capacity of the top 10 m of firn by 8 to 13% depending on the region but remained within the uncertainty intervals of our first estimations (Table 4). Additional field measurements will be needed to ascertain the infiltration ice density, its variability and its potential climatic drivers. Our definition of retention capacity assumes that retention occurs through the refreezing of meltwater and neglects potential liquid water retention seen in firn aquifer (Forster et al. 2014). Nevertheless, recent work in Southeast Greenland showed that meltwater resides less than 30 years in the aquifer before it flows into nearby crevasses and eventually leaves the ice sheet (Miller et al. 2018). On the contrary, the water refrozen within the firn is potentially retained for centuries until it is discharged through a marine terminating outlet glacier or reaches the surface in the ablation area, melts and finally runs off the ice sheet. By neglecting liquid water retention in firn, our study, in line with Harper et al. (2012), focuses on long-term meltwater retention.

3.4. Regional Climate Model performance

3.4.1. Comparison with the FAC dataset

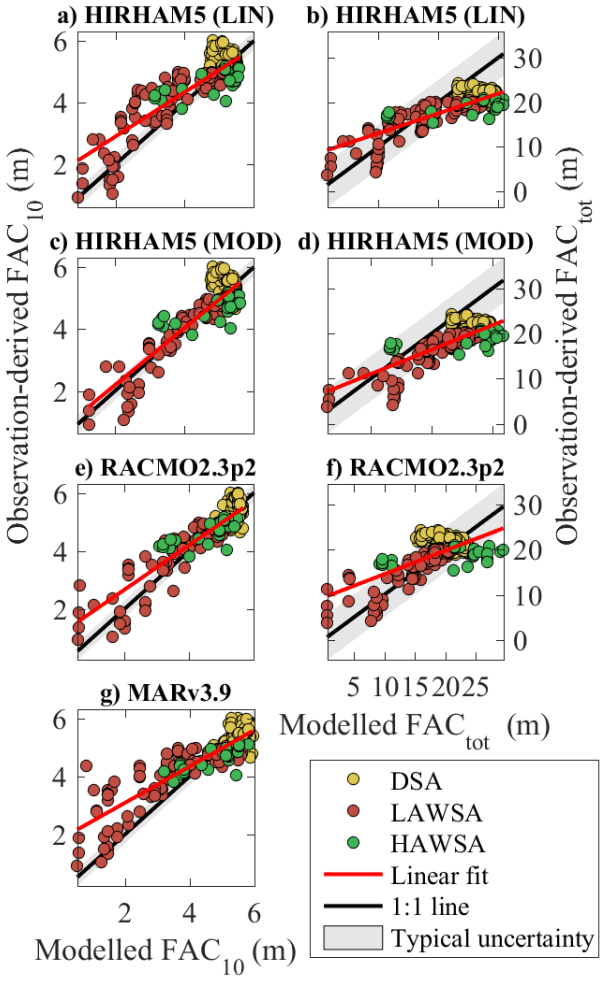

Figure 7. Comparison between the observation-derived FAC_{10} and FAC_{tot} and the simulated FAC in the corresponding cell of three RCMs.

All models reproduce the FAC_{10} observations in the DSA and HAWSA with bias ≤ 0.2 m, RMSD ≤ 0.6 m. Nevertheless, RACMO2.3p2, MARv3.9.2, and HH_LIN tend to underestimate the FAC_{10} in the LAWSA while HH_MOD did not show any bias in that area. The greater biases and RMSD regarding FAC_{tot} reflect both the performance of the RCM but also the greater uncertainty applying on our observation-derived FAC_{tot}. Overall we find that HH_MOD is the best candidate to simulate FAC_{10} and RACMO2.3p2 to simulate FAC_{tot}. Nonetheless, it appears that none of the RCMs can simultaneously

simulate both FAC_{10} and FAC_{tot} accurately, which justifies our empirical approach to map FAC_{10} and FAC_{tot} across the whole firn area.

Table 5. Performance of the RCMs for FAC_{10} and FAC_{tot}. Bias is the average difference between model and observation. RMSD stands for Root Mean Squared Error. Intercept and slopes are calculated from the linear fit between simulated and observed FAC (red line in Figure 7)

		DSA		LAWSA		HAWSA		GrIS			
	RCM	Bias (m)	RMSD (m)	Bias (m)	RMSD (m)	Bias (m)	RMSD (m)	Bias (m)	RMSD (m)	Intercept (m)	Slope (-)
FAC_{10}	HH_LIN	-0.1	0.4	-0.3	0.7	0.1	0.6	-0.2	0.6	1.5	0.7
	HH_MOD	-0.1	0.4	0.1	0.4	0.2	0.6	0.0	0.4	0.4	0.9
	RACMO2.3p2	0.1	0.3	-0.2	0.6	0.0	0.5	0.0	0.5	1.1	0.8
	MARv3.9.2	0.2	0.3	-0.3	0.9	0.2	0.5	0.0	0.6	1.8	0.6
FAC_{tot}	HH_LIN	6.4	7.1	2.7	5.3	5.6	8.3	4.9	6.6	8.6	0.4
	HH_MOD	6.5	7.2	5.3	6.2	7.0	8.9	6.1	7.0	5.6	0.5
	RACMO2.3p2	-0.4	3.3	-0.3	3.1	2.6	6.2	-0.1	3.6	9.4	0.5

3.4.2. Comparison with the spatially integrated FAC

The same pattern emerges with RCMs being able to simulate spatially integrated FAC within observational uncertainty in the DSA and underestimating it in the LAWSA. HH_MOD overestimates the spatially integrated FAC_{tot} in the DSA by 21%, leading to a 25% overestimation on the entire firn area. RACMO2.3p2 underestimates the spatially integrated FAC_{tot} by 10% in the DSA which, combined with the model's positive bias in the HAWSA, lead to a Greenland-wide estimation of spatially integrated FAC_{tot} within our observation-derived estimate's uncertainty interval.

HH_MOD uses a higher albedo than HH_LIN, and therefore calculates less surface melt and refreezing and, as a consequence, higher FAC_{10} in the LAWSA. The HH_MOD vs HH_LIN validation here confirms the sensitivity of simulated subsurface conditions, not only to the model's subsurface module but also to surface forcing (Langen et al., 2017). In a similar way, the slight negative bias in surface mass balance of RACMO2.3p2 (Noël et al. 2018), indicating excessive melt relative to snowfall, could also explain the model's underestimation of FAC_{10} in the LAWSA. Counterintuitively, HH_MOD, HH_LIN and MARv3.9.2 have in common a slight positive bias SMB (too much precipitation relative to melt) but also underestimate FAC_{10} in the LAWSA.

The way firn densification is treated in the snow models can also explain differences in simulated FAC_{10}: HIRHAM5 and MARv3.9.2 uses the same snow compaction scheme (Vionnet et al. 2012) while RACMO uses a dry compaction scheme after Kuipers Munneke et al. (2015a). HIRHAM overestimation of FAC_{tot} in the DSA arises from the relatively low firn densities modelled below ~40 m in HIRHAM, most likely because of the inadequacy of the compaction law from Vionnet et al. (2012) at depth. RACMO produces more realistic FAC_{tot} in the DSA, potentially because the densification law it uses has been tuned so that the modelled FAC matches 62 firn core observations (Kuipers Munneke et al., 2015a). Nevertheless the FAC_{tot} in the LAWSA is also underestimated by RACMO.

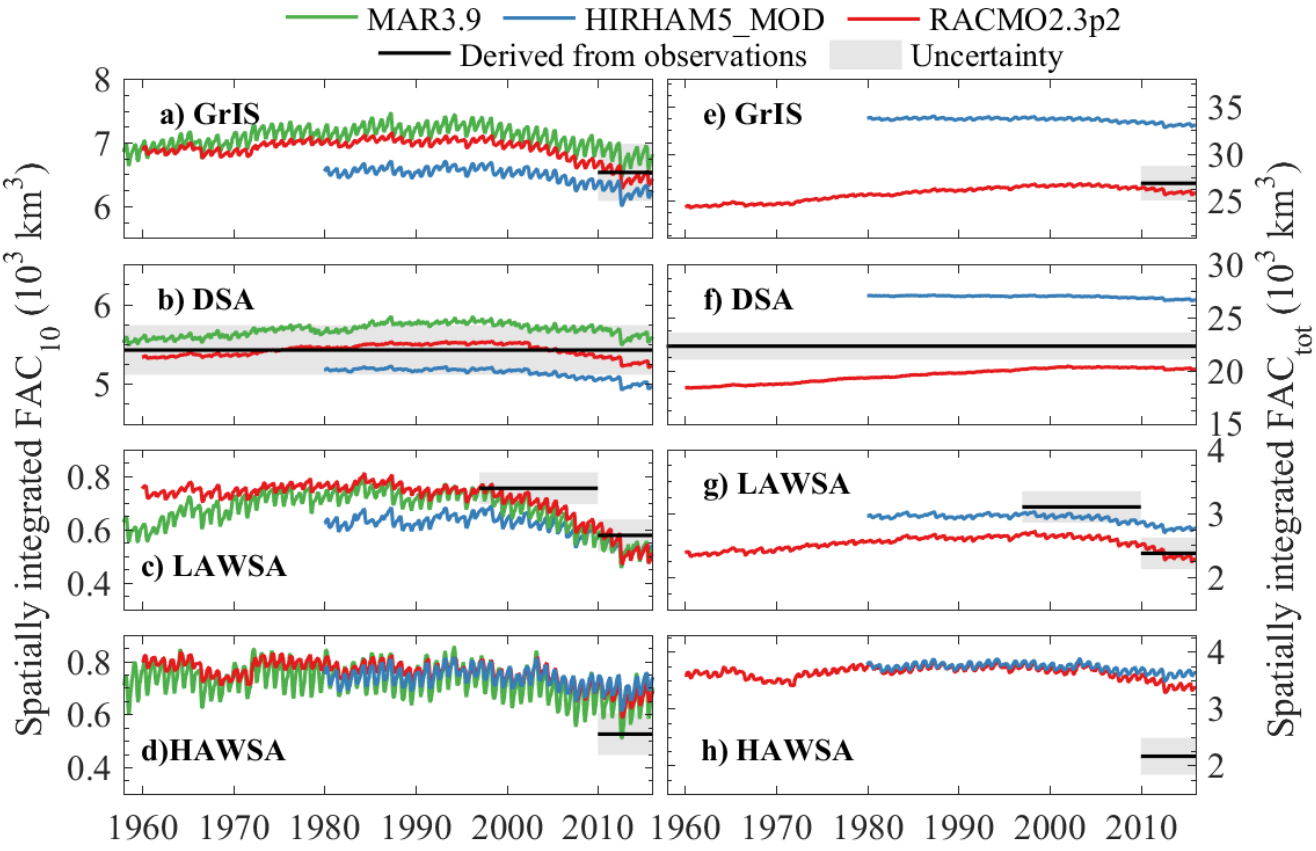

Figure 8. Temporal evolution of the FAC in the RCMs compared to the observation-derived FAC_{10} maps.

We also note that RCMs overestimate the spatially summed FAC_{10} in the HAWSA (Figure 8d) whereas they compare well with FAC_{10} observations of the HAWSA (bias ≤ 0.2 m in Table 5). It can be due to the fact that, while the RMCs reproduce the observed FAC_{10} in the interior of the HAWSA, their modelled FAC_{10} remains high in the lower HAWSA, when approaching the firn line. On the contrary, our observation-derived estimation of FAC_{10} decreases linearly with increasing with $\overline{T_a}$ and takes lower values than in the RCMs in the lower HAWSA. Nevertheless no firn observation is available in the

lower HAWSA and future FAC_{10} measurements in the HAWSA should help to know which of the RCMs or our estimation of FAC_{10} describes best in FAC_{10} the HAWSA.

Last but not least, we see that in spite of their respective biases, RCMs reproduce the decreasing FAC_{10} in the LAWSA as observed (Figure 8b). The RCMs indicate that this loss of air content was initiated in the early 2000s and accelerated in 2010 and 2012. All RCMs show a decreasing FAC_{10} in the DSA over the last two decades which contradicts with our observations (Section 3.1.1, Figure 2). This decreasing FAC_{10} could be due to the RCM missing for example an increase snowfall in the DSA which would compensate the recent warming seen in the firn area (McGrath et al., 2014; Graeter et al., 2018). Another possibility would be that the models overestimate the sensitivity of firn compaction rate to increasing temperatures.

4. Conclusions

A collection of 360 firn density profiles spanning 65 years allow us to quantify the firn air content (FAC) on the Greenland ice sheet as function of long-term air temperature and net snow accumulation averages ($\overline{T_a}$ and $\bar{\dot{b}}$). During the 2010-2017 period, we calculate that the firn layer contained 6 500 ± 450 km^3 of air in its top 10 m and 26 800 ± 1 850 km^3 within the whole firn column. We find that over the 1953-2017 period, the FAC remained constant (within measurement uncertainty) in the Dry Snow Area (DSA, where $\overline{T_a} \leq$ -19°C). In the Low Accumulation Wet Snow Area (LAWSA, where $\overline{T_a}$ > -19°C and $\bar{\dot{b}} \leq$ 600 mm w.eq. yr^{-1}), we calculate that the FAC decreased by 24 ±16 % between 1998-2008 and 2010-2017. This decreased FAC_{10} translates into the loss of meltwater retention capacity of 150 ± 100 Gt (0.4 ± 0.3 mm sea level equivalent) in the top 10m of the firn and up to 540 ± 450 Gt (1.5 ± 1.2 mm sea level equivalent) in the entire firn layer. The output from three regional climate models (HIRHAM5, RACMO2.3p2 and MAR3.9.5) indicate that our calculated decrease in FAC may have initiated in the early 2000's and accelerated in 2010 and 2012. But the mismatch between RCMs and our dataset reminds that RCMs should be used with caution when used to calculate the firn retention capacity or when converting the ice sheet's volume changes into mass changes. Finally, our study highlights the importance of in situ firn density measurements to document the evolution of the Greenland ice sheet and to improve models and sea level projections. We also illustrate how new knowledge can be gained from the synthesis of multiple data sources and encourage the scientific community to make both recent and historical data available.

5. Acknowledgement

This work is part of the Retain project funded by the Danish Council for Independent research (Grant no. 4002-00234) and the Programme for Monitoring of the Greenland Ice Sheet (www.PROMICE.dk). The FirnCover field campaigns were funded by the NASA grant NNX15AC62G. Achim Heilig was supported by DFG grant HE 7501/1-1. We thank Hubertus Fischer (Climate and Environmental Physics, University of Bern) for providing low resolution density data from firn cores

collected during the EGIG expeditions 1990 and 1992. We are grateful to Peter Langen from the Danish Meteorological Institute, Stefan Ligtenberg from the Institute for Marine and Atmospheric Research at Utrecht University (IMAU) and Xavier Fettweis from the Laboratory of Climatology, Department of Geography, University of Liège (Belgium) for providing the regional climate model output.

6. Data Availability

The FAC dataset, maps along with the firn area delineation are available at https://arcticdata.io/ and the majority of the original firn density measurements can be found in the SUMup dataset at https://doi.org/10.18739/A2JH3D23R. The source code is available at github.com/BaptisteVandecrux/FAC10_study.

7. References

Ahlstrøm, A., Gravesen, P., Andersen, S., Van As, D., Citterio, M., Fausto, R., Nielsen, S., Jepsen, H. F., Kristensen, S. S., Christensen, E. L., Stenseng, L., Forsberg, R., Hanson, S., and Petersen, D..: A new programme for monitoring the mass loss of the Greenland ice sheet, Geol. Surv. Denmark Greenland Bull., 15, 61-64, pdf, 2008.

Albert, M., and Shultz, E.: Snow and firn properties and air–snow transport processes at Summit, Greenland, Atmos. Environ., 36, 2789-2797, https://doi.org/10.1016/S1352-2310(02)00119-X, 2002.

Alley, R.: Transformations in Polar Firn, Ph.D. Thesis, University of Wisconsin, Madison, WI, USA, 1987.

Bader, H.: Sorge's law of densication of snow on high polar glaciers, J. of Glaciol. , 2, 15, 319-411, https://doi.org/10.3189/S0022143000025144, 1954.

Baker, I.: Density and permeability measurements with depth for the NEEM 2009S2 firn core, ACADIS Gateway, https://doi.org/10.18739/A2Q88G, 2012.

Benson, C. S.: Stratigraphic Studies in the Snow and Firn of the Greenland Ice Sheet, U.S. Army Snow, Ice and Permafrost Research Establishment, 1962.

Bindoff, N.L., P.A. Stott, K.M. AchutaRao, M.R. Allen, N. Gillett, D. Gutzler, K. Hansingo, G. Hegerl, Y. Hu, S. Jain, I.I. Mokhov, J. Overland, J. Perlwitz, R. Sebbari and X. Zhang: Detection and Attribution of Climate Change: from Global to Regional, in: Climate Change 2013: The Physical Science Basis.Contribution of Working Group I to the Fifth Assessment Report of the Intergovernmental Panel on Climate Change, edited by: Stocker, T.F., D. Qin, G.-K. Plattner, M. Tignor, S.K. Allen, J. Boschung, A. Nauels, Y. Xia, V. Bex and P.M. Midgley, Cambridge University Press, Cambridge, United Kingdom and New York, NY, USA, pp. 867–952, https://doi.org/10.1017/CBO9781107415324.022, 2013.

Bolzan, J. F., and Strobel, M.: Oxygen isotope data from snowpit at GISP2 Site 15., PANGAEA, https://doi.org/10.1594/PANGAEA.55511, 1999.

Box, J.: Greenland ice sheet mass balance reconstruction. Part II: Surface mass balance (1840-2010), J. Climate, 26, 6974-6989, https://doi.org/10.1175/JCLI-D-12-00518.1, 2013.

Box, J., Cressie, N., Bromwich, D. H., Jung, J.-H., van den Broeke, M. R., van Angelen, J.,Forster, R.R., Miège, C., Mosley-Thompson, E., Vinther, B., McConnell, J. R.: Greenland ice sheet mass balance reconstruction. Part I: Net snow accumulation (1600-2009), J. Climate, 26, 3919-3934, https://doi.org/10.1175/JCLI-D-12-00373.1, 2013.

Braithwaite, R., Laternser, M., and Pfeffer, W. T.: Variation of near-surface firn density in the lower accumulation area of the Greenland ice sheet, Pâkitsoq, West Greenland, J. Glaciol., 40, 136, 477-485, https://doi.org/10.3189/S002214300001234X, 1994.

Buchardt, S. L., Clausen, H. B., Vinther, B. M., and Dahl-Jensen, D.: Investigating the past and recent delta 18O-accumulation relationship seen in Greenland ice cores, Clim. Past, 8, 6, 2053-2059, https://doi.org/10.5194/cp-8-2053-2012, 2012.

Charalampidis, C., Van As, D., Box, J. E., van den Broeke, M. R., Colgan, W. T., Doyle, S. H., Hubbard, A. L., MacFerrin, M., Machguth, H. and Smeets, C. J.: Changing surface-atmosphere energy exchange and refreezing capacity of the

lower accumulation area, West Greenland, Cryosphere, 9, 6, 2163-2181, https://doi.org/10.5194/tc-9-2163-2015, 2015.

Clausen, H., Gundestrup, N. S., Johnsen, S. J., Binchadler, R., and Zwally, J.: Glaciological investigations in the Crete area, Central Greenland: a search for a new deep-drilling Site, Ann. Glaciol., 10, 10-15, https://doi.org/10.3189/S0260305500004080, 1988.

Colgan, W., Pedersen, A., Binder, D., Machguth, H., Abermann, J., and Jayred, M.: Initial field activities of the Camp Century Climate Monitoring Programme in Greenland. Geol. Surv. Denmark Greenland Bull., 41, 75-78, pdf, 2018.

de la Peña, S., Howat, I. M., Nienow, P. W., van den Broeke, M. R., Mosley-Thompson, E., Price, S. F., Mair, D., Noël, B., and Sole, A. J..: Changes in the firn structure of the western Greenland Ice Sheet caused by recent warming, Cryosphere, 9, 1203-1211, https://doi.org/10.5194/tc-9-1203-2015, 2015.

Fausto, R., Mayer, C., Ahlstrøm, A.: Satellite-derived surface type and melt area of the Greenland ice sheet using MODIS data from 2000 to 2005, Ann. Glaciol., 46, 35-42. https://doi.org/10.3189/172756407782871422, 2007.

Fausto, R. S, Andersen, S. B., Ahlstrøm, A. P., van As, D., Box, J. E., Binder, D., Citterio, M., Colgan, W., Haubner, K., Hansen, K., Karlsson, N. B., Mankoff, K. D., Pedersen, A. Ø., Solgaard, A. and Vandecrux, B.: The Greenland ice sheet – snowline elevations at the end of the melt seasons from 2000 to 2017, Geol. Surv. Denmark Greenland Bull., 41, 71-74, pdf, 2018a.

Fausto, R. S., Box, J. E., Vandecrux, B., van As, D., Steffen, K., MacFerrin, M., Machguth H., Colgan W., Koenig L. S., McGrath D., Charalampidis C. and Braithwaite, R. J.: A Snow Density Dataset for Improving Surface Boundary Conditions in Greenland Ice Sheet Firn Modeling, Front. Earth Sci., 6, 51, https://doi.org/10.3389/feart.2018.00051, 2018b.

Fettweis, X., Box, J. E., Agosta, C., Amory, C., Kittel, C., Lang, C., van As, D., Machguth, H.,, and Gallée, H.: Reconstructions of the 1900–2015 Greenland ice sheet surface mass balance using the regional climate MAR model, Cryosphere, 11, 2, 1015-1033, https://doi.org/10.5194/tc-11-1015-2017, 2017.

Fischer, H., Wagenbach, D., Laternser, M., and Haeberli, W.: Glacio-meteorological and isotopic studies along the EGIG line, central Greenland., J. of Glaciol., 41, 139, 515-527, https://doi.org/10.3189/S0022143000034857, 1995.

Forster, R. R., Box, J. E., van den Broeke, M. R., Miège, C., Burgess, E. W., Angelen, J. H.,, Lenaerts, J. T. M., Koenig, L. S., Paden, J., Lewis, C., Gogineni, S. P., Leuschen, C., and McConnell, J. R.: Extensive liquid meltwater storage in firn within the Greenland ice sheet., Nat. Geosci., 7, 95-19, https://doi.org/10.1038/NGEO2043, 2014.

Graeter, K. A., Osterberg, E., Ferris, D. G., Hawley, R. L., Marshall, H. P., Lewis, G., Meehan, T., McCarthy, F., Overly, T. and Birkel, S.D., and Birkel, S.: Ice Core Records of West Greenland Melt and Climate Forcing, Geophys. Res. Lett., 45, 7, https://doi.org/10.1002/2017GL076641, 2018.

Harper, J., Humphrey, N., Pfeffer, W. T., Brown, J., and Fettweis, X.: Greenland ice-sheet contribution to sea-level rise buffered by meltwater storage in firn, Nature, 491, 240-243, https://doi.org/10.1038/nature11566, 2012.

Hawley, R. L., Courville, Z. R., Kehrl, L., Lutz, E., Osteberg, E., Overly, T. B., and Wong, G.: Recent accumulation variability in northwest Greenland from ground-penetrating radar and shallow cores along the Greenland Inland Traverse, J. Glaciol., 60, 220, 375-382, https://doi.org/10.3189/2014JoG13J141, 2014.

Heilig, A., Eisen, O., MacFerrin, M., Tedesco, M., and Fettweis, X.: Seasonal monitoring of melt and accumulation within the deep percolation zone of the Greenland Ice Sheet and comparison with simulations of regional climate modeling, Cryosphere, 12, 1851-1866, https://doi.org/10.5194/tc-12-1851-2018, 2018.

Humphrey, N. F., Harper, J. T., and Pfeffer, W. T.: Thermal tracking of meltwater retention in Greenland's accumulation area, J. Geophys. Res., 117, F01010, https://doi.org/10.1029/2011JF002083, 2012.

Jezek, K. C.: Surface Elevation and Velocity Changes on the South Central Greenland Ice Sheet: 1980-2011 - Data Summary. BPRC Technical Report No. 2012-01, Byrd Polar Research Center, The Ohio State University, Columbus, Ohio, 2012.

Kameda, T., Narita, H., Shoji, H., Nishio, F., Fuji, Y., and Watanabe, O.: Melt features in ice cores from Site J, southern Greenland: some implication for summer climate since AD 1550, Ann. Glaciol., 21, 51-58, https://doi.org/10.3189/S0260305500015597, 1995.

Koenig, L. S., Miège, C., Forster, R. R., and Brucker, L.: Initial in situ measurements of perennial meltwater storage in the Greenland firn aquifer, Geophys. Res. Lett., 41, 81-85, https://doi.org/10.1002/2013GL058083, 2014.

Kovacs, A., Weeks, W. F., and Michitti, F.: Variation of Some Mechanical Properties of Polar Snow, Camp Century, Greenland, CRREL Res. Rpt. 276, 1969.

Kuipers Munneke, P., Ligtenberg, S. R. M., Noël, B. P. Y., Howat, I. M., Box, J. E., Mosley-Thompson, E., McConnell, J. R., Steffen, K., Harper, J. T., Das, S. B., and van den Broeke, M. R.: Elevation change of the Greenland Ice Sheet due to surface mass balance and firn processes, 1960–2014, Cryosphere, 9, 2009–2025, https://doi.org/10.5194/tc-9-2009-2015, 2015a.

Kuipers Munneke, P., Ligtenberg, S.R., Suder, E.A. and van den Broeke, M.R.: A model study of the response of dry and wet firn to climate change. Ann. Glaciol., 56(70), pp.1-8, https://doi.org/10.3189/2015AoG70A994, 2015b.

Langen, P., Fausto, R. S., Vandecrux, B., Mottram, R., and Box, J.: Liquid Water Flow and Retention on the Greenland Ice Sheet in the Regional Climate Model HIRHAM5: Local and Large-Scale Impacts., Front. Earth Sci., 4, 110, https://doi.org/10.3389/feart.2016.00110, 2017.

Langway, C. C.: Stratigraphic analysis of a deep ice core from Greenland, CRREL Res. Rpt. 77, 1967.

Ligtenberg, S. R., Kuipers Munneke, P., Noël, B. P., and . van den Broeke, M.: Improved simulation of the present-day Greenland firn layer (1960–2016), Cryosphere, https://doi.org/10.5194/tc-12-1643-2018, 2018.

Lomonaco, R., Albert, M., and Baker, I.: Microstructural evolution of fine-grained layers through the firn column at Summit, Greenland, J. Glaciol., 57, 204, https://doi.org/10.3189/002214311797409730, 2011.

Lucas-Picher, P., Wulff-Nielsen, M., Christensen, J. H., Aðalgeirsdóttir, G., Mottram, R., and Simonsen, S.: Very high resolution in regional climate model simulations for Greenland: Identifying added value, J. Geophys. Res., 117, D02108, https://doi.org/10.1029/2011JD016267, 2012.

Machguth, H., MacFerrin, M., As, D. v., Box, J., Charalampidis, C., Colgan, W., Fausto, R.S., Meijer, H.A., Mosley-Thompson, E. and van de Wal, R.S.: Greenland meltwater storage in firn limited by near-surface ice formation, Nature Clim. Change, 6, 390-395, https://doi.org/10.1038/NCLIMATE2899, 2016.

Mayewski, P., and Whitlow, S.: 2016. Snow Pit and Ice Core Data from Southern Greenland, 1984, NSF Arctic Data Center. https://doi.org/10.5065/D6S180MH, 2016.

Mayewski, P., and Whitlow S.: Snow Pit Data from Greenland Summit, 1989 to 1993. NSF Arctic Data Center. https://doi.org/10.5065/D6NP22KX, 2016.

Miège, C., Forster R.C., B. J., Burgess, E., McConnell, J., Pasteris, D., and Spikes, V. B.: Southeast Greenland high accumulation rates derived from firn cores and ground-penetrating radar, Ann. Glaciol., 54, 63, 322-332, https://doi.org/10.3189/2013AoG63A358, 2013.

Montgomery, L., Koenig, L., and Alexander, P.: The SUMup dataset: compiled measurements of surface mass balance components over ice sheets and sea ice with analysis over Greenland, Earth Syst. Sci. Data, 10, 1959-1985, https://doi.org/10.5194/essd-10-1959-2018, 2018.

Morris, E. M., and Wingham, D. J.: Densification of polar snow: Measurements, modeling and implication for altimetry, J. Geophys. Res.-Earth, https://doi.org/10.1002/2013JF002898, 2014.

Mosley-Thompson, E., McConnell, J., Bales, R., Li, Z., Lin, P.-N., and Steffen, K.: Local to regional-scale variability of annual net accumulation on the Greenlandice sheet from PARCA cores, J. Geophys. Res., 106, 33839–33851, https://doi.org/10.1029/2001JD900067, 2001.

Mote T. L.: Greenland surface melt trends 1973–2007: Evidence of a large increase in 2007, Geophys. Res. Lett., 34(22), https://doi.org/10.1029/2007GL031976, 2007.

Nerem R. S., Beckley B. D., Fasullo J. T., Hamlington B. D., Masters D, Mitchum G. T.: Climate-change–driven accelerated sea-level rise detected in the altimeter era. P. Natl. Acad. Sci. U.S.A., 7:201717312, https://doi.org/10.1073/pnas.1717312115, 2018.

Nghiem, S.V., Hall, D.K., Mote, T.L., Tedesco, M., Albert, M.R., Keegan, K., Shuman, C.A., DiGirolamo, N.E. and Neumann, G.: The extreme melt across the Greenland ice sheet in 2012, Geophys. Res. Lett., 39, L20502, https://doi.org/10.1029/2012GL053611, 2012.

Noël, B., van de Berg, W. J., van Wessem, J. M., van Meijgaard, E., van As, D., Lenaerts, J. T. M., Lhermitte, S., Kuipers Munneke, P., Smeets, C. J. P. P., van Ulft, L. H., van de Wal, R. S. W., and van den Broeke, M. R.: Modelling the climate and surface mass balance of polar ice sheets using RACMO2 – Part 1: Greenland (1958–2016), The Cryosphere, 12, 811-831, https://doi.org/10.5194/tc-12-811-2018, 2018.

Porter, S., and Mosley-Thompson, E.: Exploring seasonal accumulation bias in a west central Greenland ice core with observed and reanalyzed data, J. Glaciol., 60, 224, 1065-1074, https://doi.org/10.3189/2014JoG13J233, 2014.

Reed, S.: Performance Study of the Dewline Ice Cap Stations, 1963, CRREL Special Report 72, 1966.

Renaud, A.: Etude physiques et chimiques sur la glace de l'inlandsis du Groenland , Medd. Groenland, 2, 177, 100-107, 1959.

Shumskii P.A.: Principles of structural glaciology: the petrography of fresh-water ice as a method of glaciological investigation. Dover Publications Inc..1964.

Simonsen, S.B., Stenseng, L., Aðalgeirsdóttir, G., Fausto, R.S., Hvidberg, C.S. and Lucas-Picher, P.: Assessing a multilayered dynamic firn-compaction model for Greenland with ASIRAS radar measurements. J. Glaciol., 59(215), pp.545-558, https://doi.org/10.3189/2013JoG12J158, 2013.

Spencer, M. K., Aller, R. B., and Creyts, T. T.: Preliminary firn-densification model with 38-site dataset, J. Glaciol., 47, 159, 671-676, https://doi.org/0.3189/172756501781831765, 2001.

Steen-Larsen, H.C., Masson-Delmotte, V., Sjolte, J., Johnsen, S.J., Vinther, B.M., Bréon, F.M., Clausen, H.B., Dahl-Jensen, D., Falourd, S., Fettweis, X. and Gallée, H.: Understanding the climatic signal in the water stable isotope records from the NEEM cores, J. Geophys. Res., 116, D06108, https://doi.org/10.1029/2010JD014311, 2011.

Sørensen, L. S., Simonsen, S.B., Nielsen, K., Lucas-Picher, P., Spada, G., Adalgeirsdottir, G., Forsberg, R. and Hvidberg, C.: Mass balance of the Greenland ice sheet (2003–2008) from ICESat data–the impact of interpolation, sampling and firn density. Cryosphere, 5, pp.173-186, https://doi.org/ 10.5194/tc-5-173-2011, 2011.

Vallelonga, P., Christianson, K., Alley, R. B., Anandakrishnan, S., Christian, J. E. M., Dahl-Jensen, D., Gkinis, V., Holme, C., Jacobel, R. W., Karlsson, N. B., Keisling, B. A., Kipfstuhl, S., Kjær, H. A., Kristensen, M. E. L., Muto, A., Peters, L. E., Popp, T., Riverman, K. L., Svensson, A. M., Tibuleac, C., Vinther, B. M., Weng, Y., and Winstrup, M.: Initial results from geophysical surveys and shallow coring of the Northeast Greenland Ice Stream (NEGIS), Cryosphere, 8, 1275-1287, https://doi.org/10.5194/tc-8-1275-2014, 2014.

van Angelen, J., Lenaerts, J. T., van den Broeke, M. R., Fettweis, X., and van Meijgaard, E.: Rapid loss of firn pore space accelerates 21st century Greenland mass loss, Geophys. Res. Lett., 40, 2109-2113, https://doi.org/10.1002/grl.50490, 2013.

Vandecrux, B., Fausto, R.S., Langen, P.L., Van As, D., MacFerrin, M., Colgan, W.T., Ingeman-Nielsen, T., Steffen, K., Jensen, N.S., Møller, M.T. and Box, J.E.. Drivers of Firn Density on the Greenland Ice Sheet Revealed by Weather Station Observations and Modeling, J. Geophys.l Res.-Earth, https://doi.org/10.1029/2017JF004597, 2018.

van den Broeke, M. R., Enderlin, E. M., Howat, I. M., Kuipers Munneke, P., Noël, B. P. Y., van de Berg, W. J., van Meijgaard, E., and Wouters, B.: On the recent contribution of the Greenland ice sheet to sea level change, Cryosphere, 10, 1933-1046, https://doi.org/10.5194/tc-10-1933-2016, 2016.

van der Veen, C. J., Mosley-Thompson, E., Jezek, K. C., Whillans, I. M., and Bolzan, J. F.: Accumulation rates in South and Central Greenland, Polar Geography, 25, 2, 79-162, https://doi.org/10.1080/10889370109377709, 2001.

Wilhelms, F.: Measuring the Conductivity and Density of Ice Cores, Ber. Polarforsch., 191, 1996.

Firn data compilation reveals the evolution of the firn air content on the Greenland ice sheet

Baptiste Vandecrux[1,2], Michael MacFerrin[3], Horst Machguth[4, 5], William T. Colgan[1], Dirk van As[1], Achim Heilig[6], C. Max Stevens[7], Charalampos Charalampidis[8], Robert S. Fausto[1], Elizabeth M. Morris[9], Ellen Mosley-Thompson[10], Lora Koenig[11], Lynn N. Montgomery[11], Clément Miège[12], Sebastian B. Simonsen[13], Thomas Ingeman-Nielsen[2], Jason E. Box[1]

[1] Department of Glaciology and Climate, Geological Survey of Denmark and Greenland, Copenhagen, Denmark.
[2] Department of Civil Engineering, Technical University of Denmark, Lyngby, Denmark.
[3] Cooperative Institute for Research in Environmental Sciences, University of Colorado, Boulder, CO USA
[4] Department of Geosciences, University of Fribourg, Fribourg, Switzerland
[5] Department of Geography, University of Zurich, Zurich, Switzerland
[6] Department of Earth and Environmental Sciences, LMU, Munich, Germany
[7] Department of Earth and Space Sciences, University of Washington, WA USA
[8] Bavarian Academy of Sciences and Humanities, Munich, Germany
[9] Scott Polar Research Institute, Cambridge University, United Kingdom
[10] Byrd Polar and Climate Research Center and Department of Geography, Ohio State University, Columbus, OH USA.
[11] National Snow and Ice Data Center, University of Colorado, Boulder, CO, United States
[12] Department of Geography, Rutgers University, Piscataway, NJ, United States
[13] DTU Space, National Space Institute, Department of Geodynamics, Technical University of Denmark, Kgs. Lyngby, Denmark

Correspondence to: B. Vandecrux (bava@byg.dtu .dk)

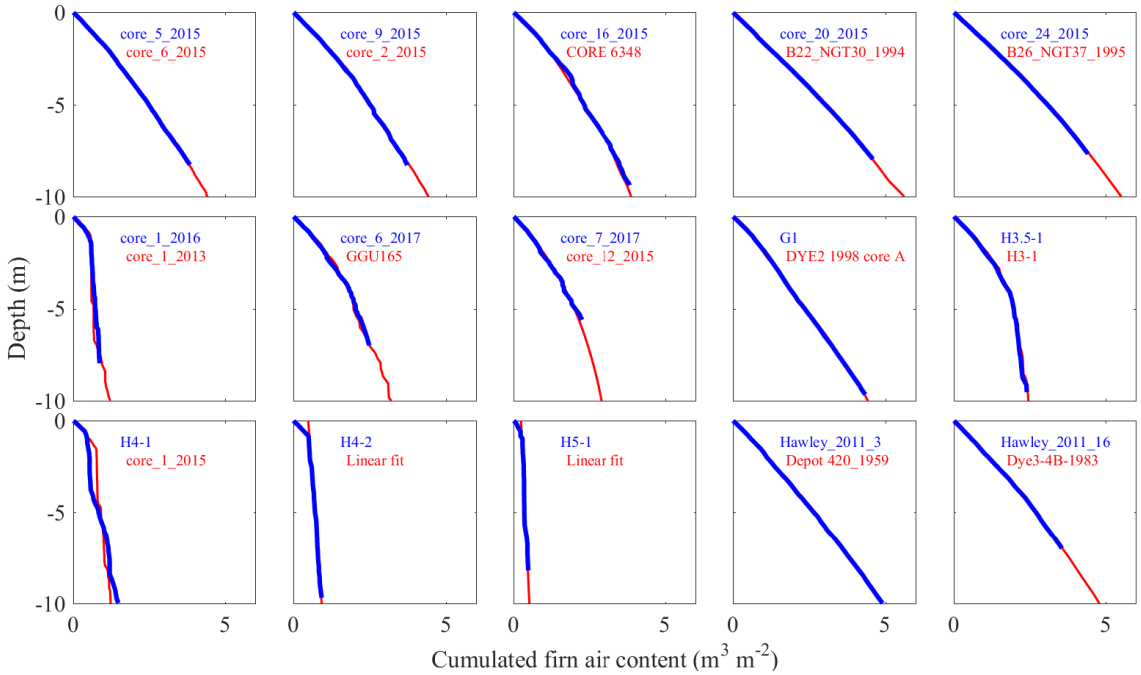

Figure S1. Extrapolation of FAC to 10 m using the lower section of the existing 10 m-long FAC profile that has the lowest Root Mean Squared Difference with the shallow FAC profile.

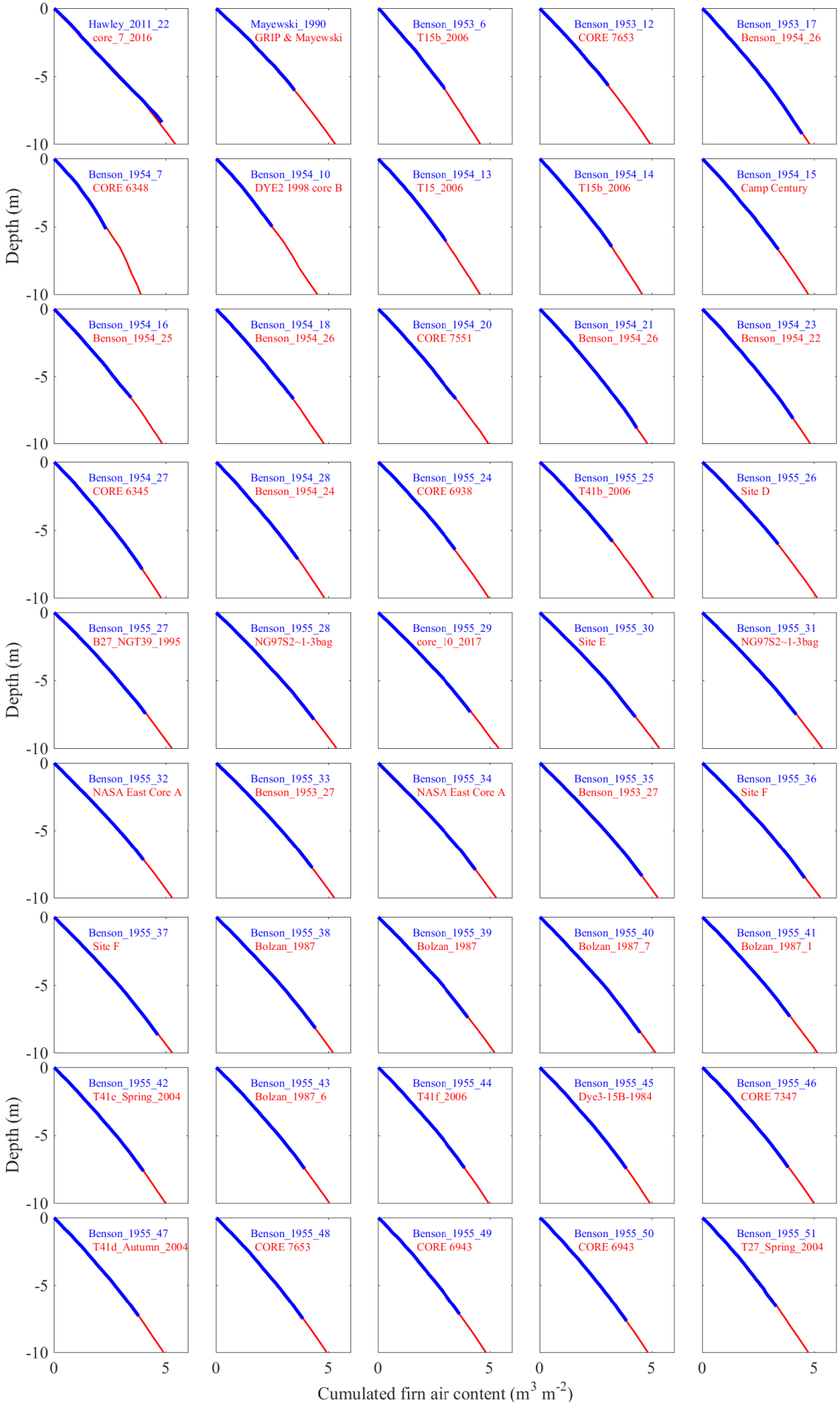

Figure S1. Extrapolation of FAC to 10 m using the lower section of the existing 10 m-long FAC profile that has the lowest Root Mean Squared Difference with the shallow FAC profile.

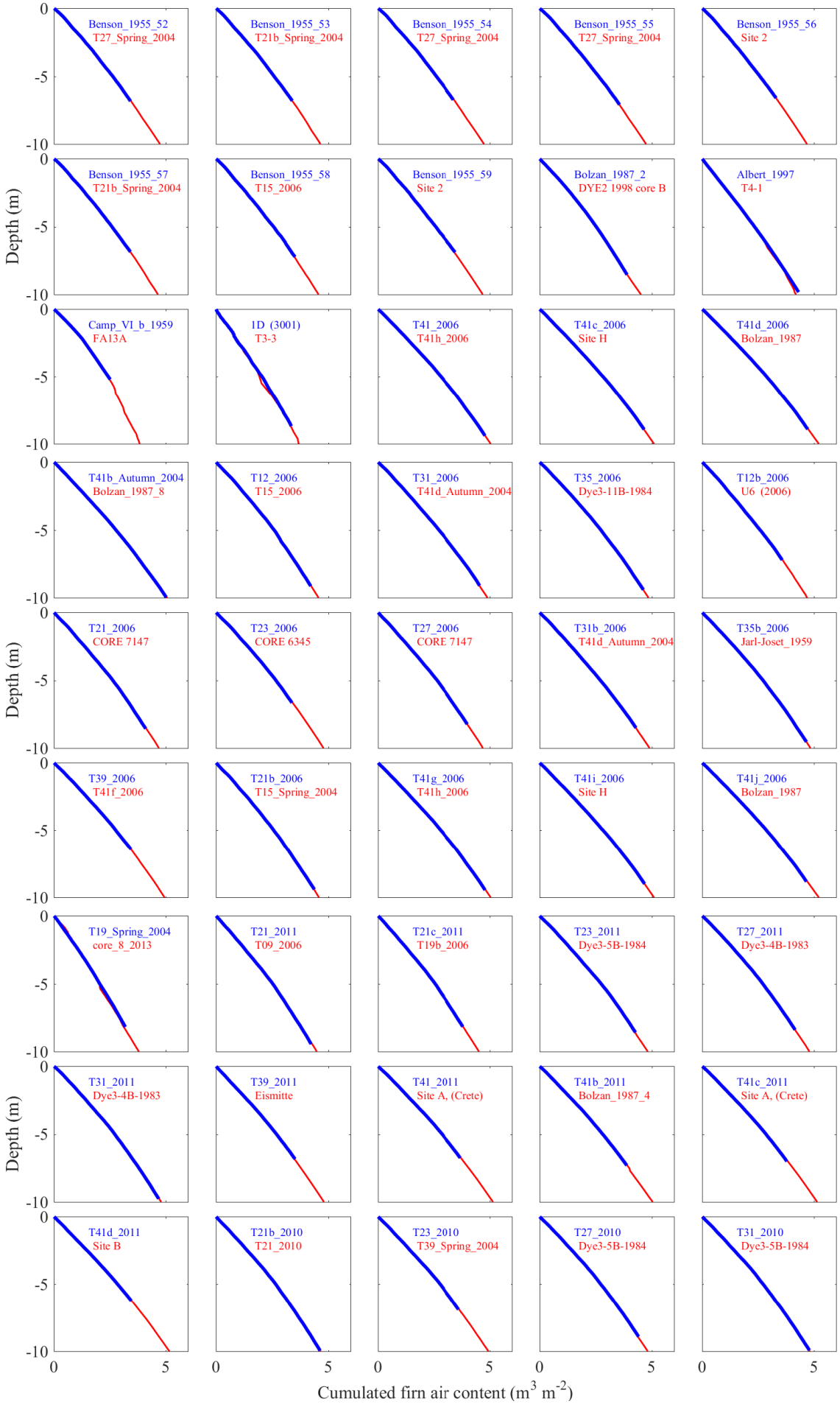

Figure S1. Extrapolation of FAC to 10 m using the lower section of the existing 10 m-long FAC profile that has the lowest Root Mean Squared Difference with the shallow FAC profile.

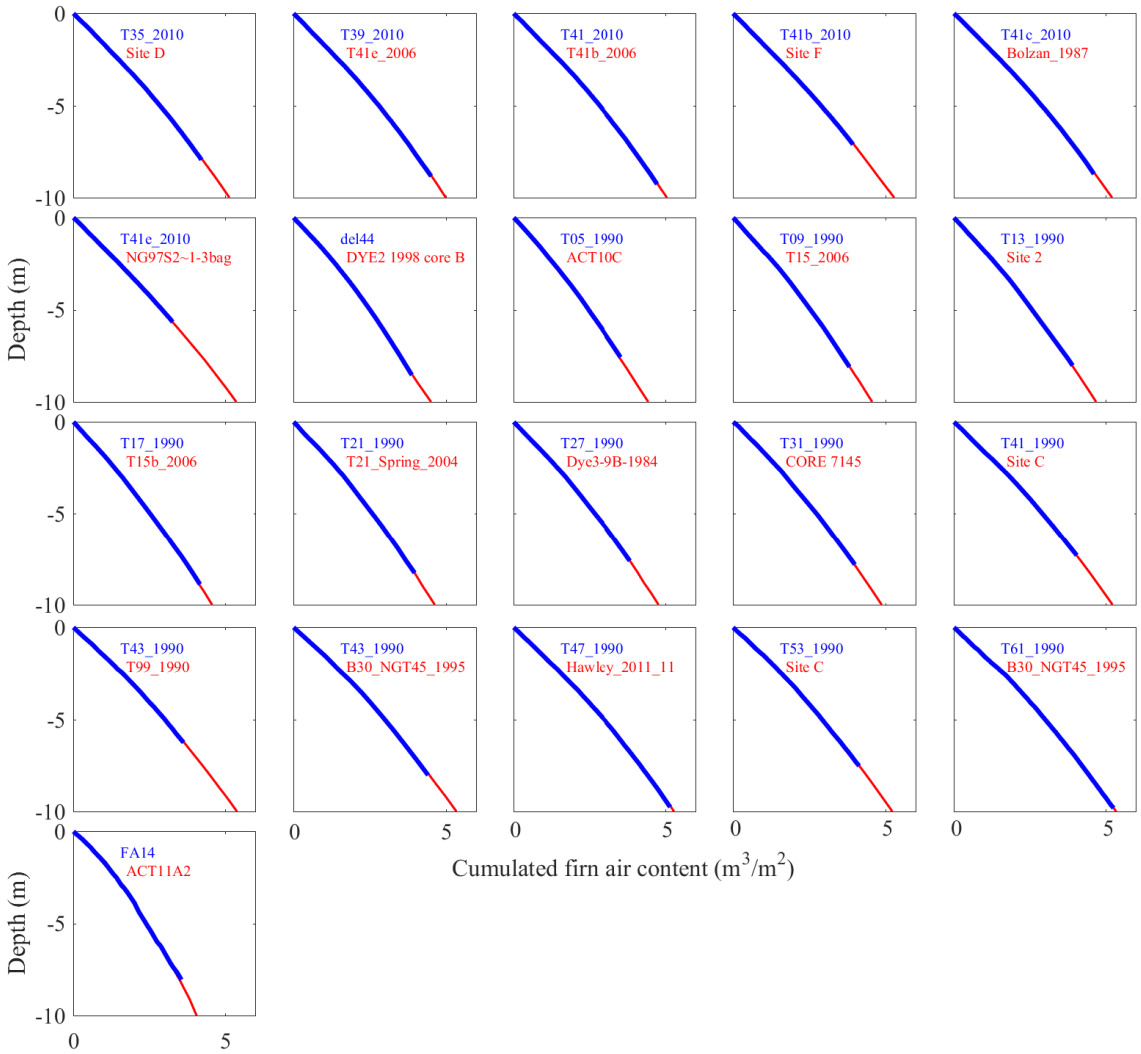

Figure S1. Extrapolation of FAC to 10 m using the lower section of the existing 10 m-long FAC profile that has the lowest Root Mean Squared Difference with the shallow FAC profile.

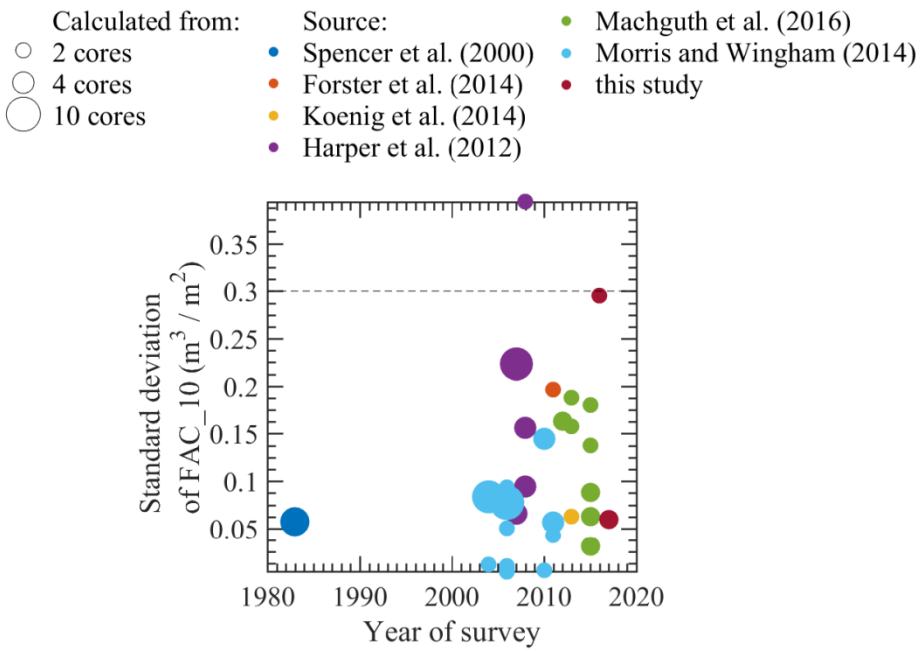

Figure S2. Standard deviation of FAC measurements located within 1 km. Dashed line indicate 0.3 m^3 m^{-2}, value used to describe the uncertainty applying on any FAC_{10} measurement.

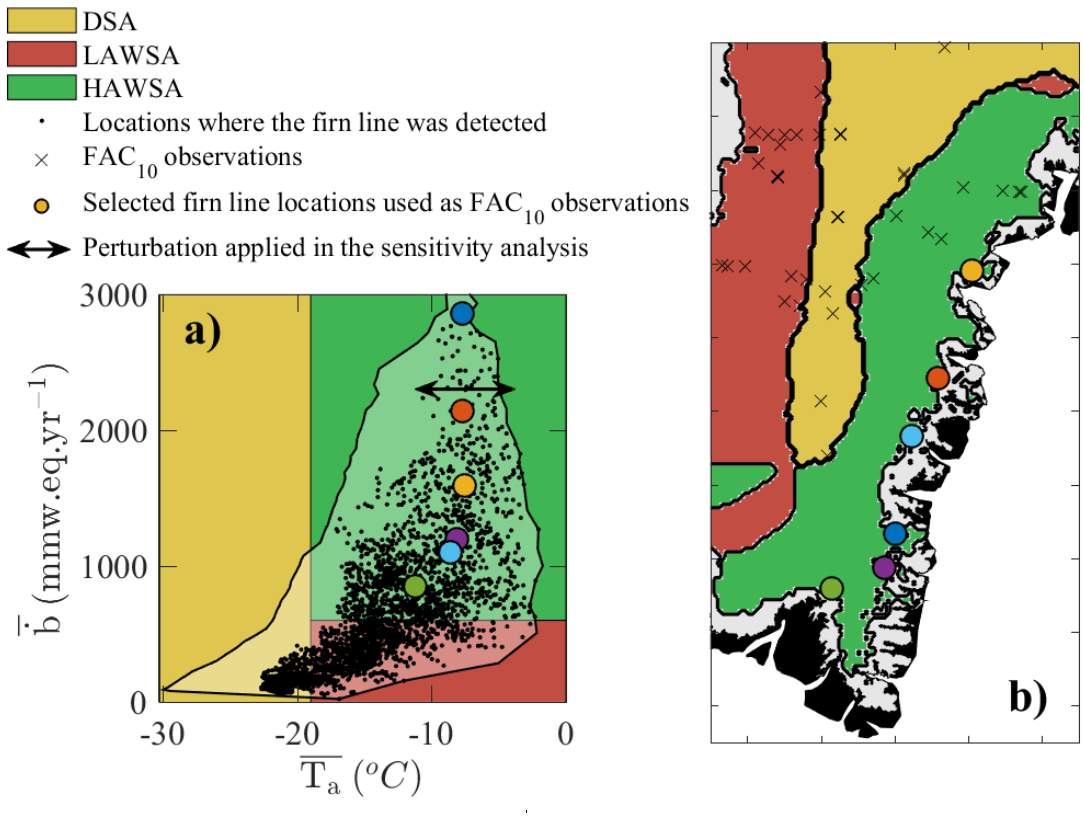

Figure S3. Selection of remotely-sensed firn line locations in the HAWSA to be used as FAC10 observations. a) Remotely-sensed firn line locations in the temperature-accumulation space ($\overline{T_a}$, $\overline{\dot{b}}$). b) Locations selected from the remotely-sensed firn line.

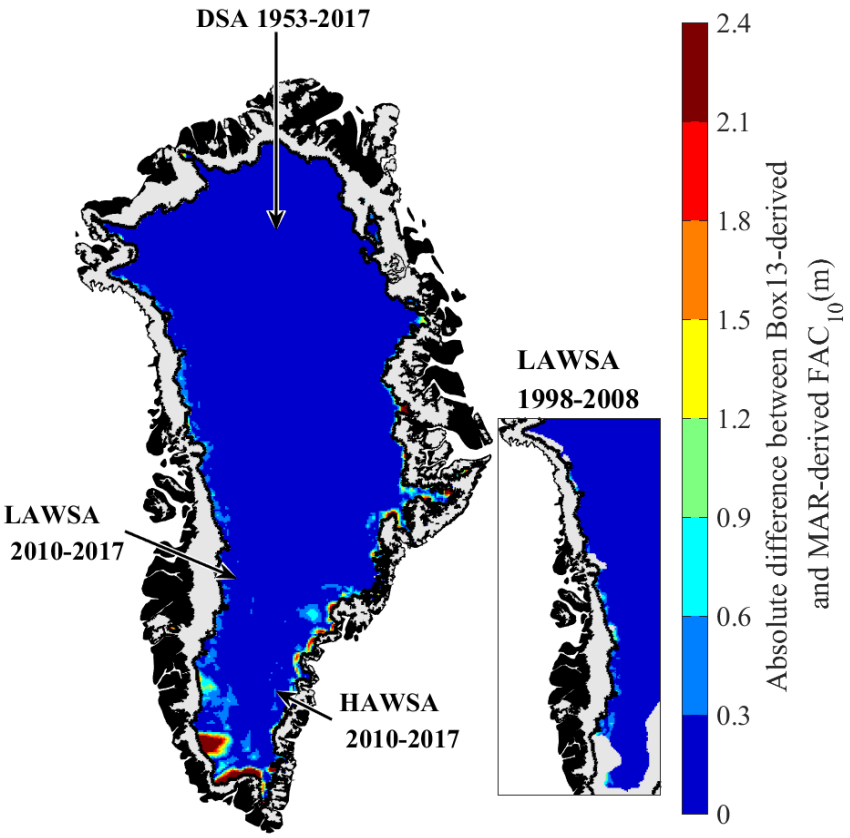

Figure S4. Difference between the FAC_{10} maps obtained using $\overline{\dot{b}}$ and $\overline{T_a}$ from Box (2013) and Box et al. (2013) and the maps obtained using $\overline{\dot{b}}$ and $\overline{T_a}$ from MAR (Fettweis et al. 2017).